Available online at www.sciencedirect.com

ScienceDirect

Current Opinion in Biotechnology

Review

In-situ product recovery in microfluidic bioreactors

Corinna Golze[1,#], Claudia Hackl[1,2,#], Alexander Grünberger[3] and Andreas Schmid[1]

Microfluidic reaction formats are of increasing importance to produce low molecular weight chemicals. *In-situ* product recovery in such systems benefits from intrinsic physical advantages of microfluidics, including increased mass and energy transfer and continuous processing. This opinion highlights the design space for microfluidic *in-situ* recovery of gaseous products with respect to rates of production and product recovery, as well as physical constraints limiting product titers. In a theoretical case study, O_2 produced by cyanobacteria in a microfluidic reactor is used to benchmark productivities through process simulations. In general, the productivity of microfluidic bioprocesses is confined by biocatalytic reaction rates, diffusion rates, and residence time. Key challenges for scale-up, and thus achieving high space-time yields, comprise biocatalyst formats, catalytic robustness, and specific turn-over rates, as well as numbering-up of microfluidic devices. Economically and physically accessible application areas may thus be limited to milligram or higher gram quantities of specialty products.

Addresses
[1] Helmholtz Center for Environmental Research (UFZ), Solar Materials Biotechnology, Leipzig 04318, Germany
[2] Leibniz Institute of Surface Engineering (IOM), Biocompatible and Bioactive Surfaces, Leipzig 04318, Germany
[3] Karlsruhe Institute of Technology (KIT), Microsystems in Bioprocess Engineering, Karlsruhe 76131, Germany

Corresponding author: Schmid, Andreas (andreas.schmid@ufz.de)
[#] These authors contributed equally.

Current Opinion in Biotechnology 2026, **99**:103498

This review comes from a themed issue on **Nanobiotechnology**

Edited by **Jean-Loup Faulon** and **Olivier Borkowski**

Available online xxxx

https://doi.org/10.1016/j.copbio.2026.103498

Introduction

Most microbial production processes are conducted in (fed-)batch mode at higher m^3 scales. Continuous bioprocesses, by contrast, enable superior control of reaction conditions and, particularly at the microscale, provide enhanced mixing and improved mass and heat transfer. This motivated the development of solutions for unstable, inhibiting, or toxic reactants via *in-situ* product recovery (ISPR) strategies for the bioproduction of low molecular weight compounds [1–4]. Here, we focus on continuous microfluidic reactors [5] and define ISPR as product recovery occurring directly at the site and time of formation, excluding configurations in which product separation is spatially or temporally decoupled from the reaction. Particularly, we analyze the integration of whole-cell biocatalysis with ISPR as an initial downstreaming step, emphasizing aqueous-gas phase microfluidic bioprocesses. Despite clear conceptual advantages, practical implementations remain scarce due to narrow process windows and the need to simultaneously balance reaction kinetics, mass transfer, and diffusion with permeability constraints of materials separating reaction and product recovery compartments. We move beyond qualitative assessments by introducing a quantitative process window framework that explicitly couples specific activity, production, and ISPR rates with geometry-defined residence times, enabling systematic identification of biocatalytic reactions and operating regimes that are intrinsically compatible with microfluidic ISPR (μ-ISPR), providing a rational basis for reactor and process design. The μ-ISPR process window reveals that, particularly in nanobiotechnology, product formation rates defined by synthetic biology have to be well balanced with material-dependent non-biological product recovery rates to maximize overall process efficiencies.

Physics of microfluidic systems

Microfluidic devices are becoming increasingly important for developing bioprocesses. In analytical settings, biocatalyst kinetics and stability are evaluated [6]. Microfluidics for preparative bioprocesses necessitate scale-up solutions and innovative process strategies, including product recovery to achieve relevant product amounts (Figure 1). The main benefit of microfluidics is the highly increased surface-to-volume ratio (SVR) ranging from 10^4 m^2/m^3 to 10^5 m^2/m^3 for channel diameters of 40 μm to 400 μm, irrespective of the channel length, in contrast to standard tank reactors with SVR < 10 m^2/m^3 [7]. Consequently, the advantages include fast heat and mass transfer. With Reynolds numbers typically below 10 [8], the flow in microfluidics is laminar (Stokes flow). Mixing is then solely diffusion-driven as described by Fick's law, while diffusion

Figure 1

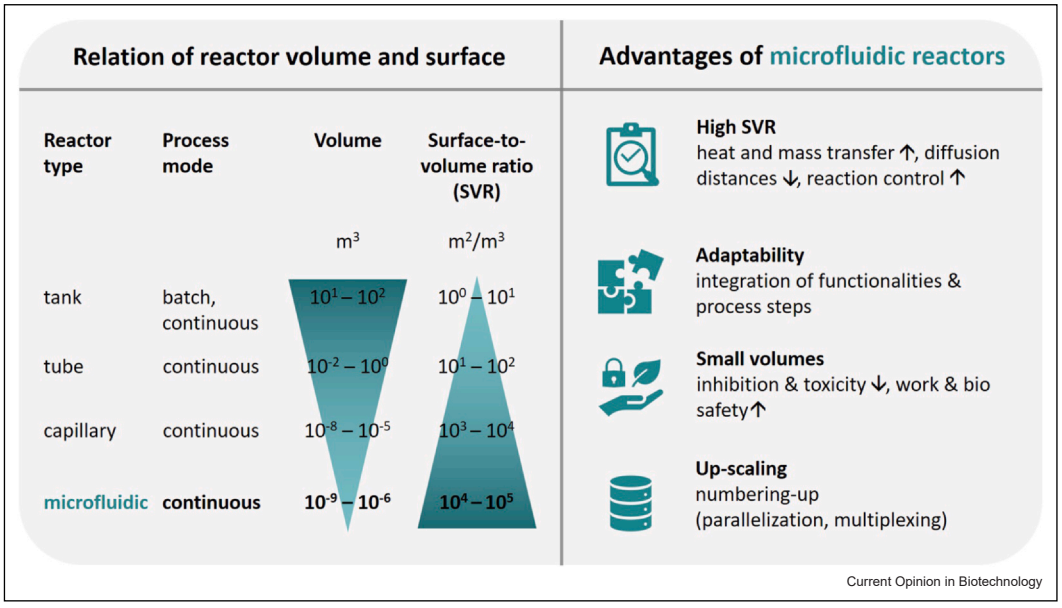

Schematic overview illustrating the correlation between reactor volumes and surfaces for bioreactor types of varying dimensions, highlighting the advantages of microfluidic chips as a reaction format. The calculations were conducted using typical reactor diameters: tube reactor 10–60 mm [16], capillary reactor 0.5–3 mm, microfluidic reactor 50–500 µm [17].

distances remain short in the narrow channels, enabling precise flow and tight environmental and reaction control. Effective passive and low-energy microfluidic mixing can be achieved using droplet or segmented flow, where Taylor-type convection, in addition to diffusion, significantly enhances mass transfer [9]. Volumes handled in microfluidics are in the µL to low mL range, which reduces costs, energy consumption, and the use of (hazardous) chemicals while increasing work- and bio-safety. Thus, otherwise unfeasible bioprocesses can be performed at the microscale. However, they are limited by the total product mass set by space-time yields and retention times. A unique feature of microfluidic devices is their adaptability, allowing integration of different functionalities and complex (bio)process steps, including ISPR, within a single device. Bioprocesses limited by inhibition or toxic by-products benefit particularly from integration into continuous microfluidic reactors [10]. This advantageous shift of the reaction equilibrium towards product formation can be significantly enhanced by µ-ISPR as demonstrated for liquid–liquid extraction [11–13] and membrane-based approaches [14, 15]. Integrating bioprocesses and ISPR into microfluidic systems can enhance recovery efficiencies, since recovery rates are governed mainly by diffusion of the target molecules, product concentration, and material properties. Consequently, product formation and recovery rates must be balanced in preparative microfluidic bioprocesses.

Productive microsystems

Microfluidics is expanding from an analytical tool for process design towards a 'transformative platform' enabling continuous flow biocatalysis and fermentation [18–20]. Process productivity is determined by space-time yields, based on volumetric reaction rates and biocatalyst amounts per volume. Recent studies highlight whole-cell microfluidic systems, which benefit from high SVRs, enhanced mass transfer, and increased overall productivity [19, 21–23] (Table S1). Hoschek et al. increased space-time yields by using high densities of whole-cell biocatalysts in a capillary biofilm reactor [17]. Kronstadt et al. used mesenchymal stem cells for extracellular vesicle production within a continuous microfluidic 3D scaffold-perfusion system, reaching an up to 80-fold higher yield at analytical scale compared to conventional shaking flasks [24]. Lemke et al. introduced a polydimethylsiloxane (PDMS)-glass microbioreactor for flow-induced *Escherichia coli* immobilization, preventing shear-related bioactivity loss and enabling continuous 4-vinylphenol production with extrapolated space–time yields of 6000–8000 $g \cdot L^{-1} \cdot d^{-1}$ for up to 50 hours, corresponding to over 40 $mmol \cdot L^{-1} \cdot min^{-1}$, before a sharp decline from limited catalytic robustness [25]. Assuming ideal robustness, numbering up with only 90 bioreactors would yield 1 $kg \cdot d^{-1}$ of product. Another study of Bajić et al. achieved a maximum volumetric productivity of 2.23 $mmol \cdot L^{-1} \cdot min^{-1}$ for L-erythrulose from *E. coli* in a hydrogel microreactor, adaptable to different whole-cell

and enzymatic reactions [26]. These pioneering studies demonstrate the potential of microfluidic whole-cell biocatalysis by leveraging its key advantages (Figure 1). Product amounts per hour (Table S1) span several orders of magnitude, ranging from nanograms (chiral 5-nitro-2,8-nonanediol [23]) to milligrams (L-malic acid [22], 4-vinylphenol [25]), and several grams (L-erythrulose [26], neurotransmitter γ-aminobutyric acid [21]). Further research is crucial for developing these laboratory examples towards commercial competitiveness.

Downstreaming in capillaries and microfluidics

Microscale downstreaming processes provide technically and economically viable options for unstable, toxic, or low-yield products [27]. Microfluidic platforms enable seamless ISPR integration, yet this potential is largely untapped [13, 28]. High SVRs govern interphase mass transfer, product yield, and reaction environment, favoring techniques like aqueous two-phase systems (ATPS) [29] and pervaporation [30]. The latter facilitates liquid–gas separation via membrane mass transfer [31]. Proof-of-concept studies demonstrated high recovery efficiencies at the microscale. Zhang et al. achieved > 80% acetone recovery using a glass chip with thin PDMS membranes (< 150 µm), with mass transfer limitations shifting from liquid-phase at low membrane thickness to membrane diffusion at higher thickness. Thus, narrow channels and thin membranes proved advantageous [14]. Ziemecka et al. modeled vacuum- and purge gas-driven methanol pervaporation in a PDMS-based chip with 100–120 µm membranes, reaching 79% (vacuum) and 94% (purge gas) efficiencies by optimizing pressure, temperature, permeability, and flow rate. High efficiencies depended on maximizing membrane permeability, lowering membrane thickness, and flow rates while optimizing channel geometry [32]. An open PDMS-based membrane system for ethanol removal from radiopharmaceuticals was described by Zizzari et al. and achieved < 40% to 95% efficiencies depending on operating conditions, with SVR showing the strongest influence, followed by residence time over temperature [33]. Potočnik et al. introduced a 3D-printed chip with an integrated PDMS membrane (300 µm) for vacuum-driven pervaporation, enabling up to 97% recovery efficiency for different volatile organic compounds, with membrane diffusion dominating mass transfer due to material properties and geometry [15]. These studies highlight the potential of microscale downstreaming while emphasizing the complex interplay of parameters (channel geometry, membrane properties, mass transfer mechanisms) for efficient product recovery. Membrane integration broadens bioreactor geometries and enables application of non-compatible phases through physical separation, though membrane diffusion remains the main limitation.

Furthermore, initial studies demonstrated µ-ISPR in fermentations. Wahab et al. introduce a PDMS-based microfluidic device featuring chemostat, lysis, and ATPS modules yielding green fluorescent protein with *E. coli* at a recovery efficiency of around 74% [34]. High-cell-density cultivation of *Nostoc*, *Anabaena*, and *Pseudomonas* in a polystyrene-capillary biofilm photobioreactor to produce H_2 was investigated by Toepel et al. Slug-flow gas phase integration enabled *in-situ* H_2 recovery up to 300 µmol $H_2 \cdot L^{-1} \cdot h^{-1}$ [35].

Potential applications of ISPR in productive microsystems

Process intensification by µ-ISPR can be benchmarked by defining process windows [5] linking feasible reactor designs [36] with economically viable operating conditions [37]. ISPR is beneficial when the product removal rate $r_{removal}$ equals or exceeds the product formation rate $r_{production}$, that is, $r_{removal} \geq r_{production}$ (Figure 2). If $\frac{r_{removal}}{r_{production}} \geq 1$, the product is completely removed from the reaction space. If $\frac{r_{removal}}{r_{production}} < 1$, product accumulates and the ISPR potential is not fully exploited, which is particularly disadvantageous for inhibitory products. Volumetric productivity $r_{productivity}^{volumetric}$ of a bioprocess depends on cell density and specific activity, with optimal cell densities of industrial processes ranging from 5 g_{CDW}/L to 75 g_{CDW}/L [38]. We categorize reactions with a specific activity of 10^4 to 10^5 µmol·min^{-1}·g_{CDW}^{-1} as fast and those with a specific activity of 10^0 to 10^2 µmol·min^{-1}·g_{CDW}^{-1} as slow. Corresponding volumetric productivities range from 5 µmol·min^{-1}·L^{-1} to 7.5 mmol·min^{-1}·L^{-1} (slow) and from 0.05 to 7.5 mol·min^{-1}·L^{-1} (fast). While fast reactions are mainly of academic interest, they are difficult to scale, and production remains at laboratory scale (< 10 L). Industrial bioprocesses typically achieve stable volumetric productivities ranging from 0.01 to 20 mmol·min^{-1}·L^{-1} [38, 39].

We now focus on whole-cell biocatalysis involving gaseous or volatile products, like O_2 and H_2 (photosynthesis), CO_2 (respiration), volatile hydrocarbons, alcohols, terpenes, and NH_3. ISPR via membrane-based gas separation or pervaporation offers a gentle, economical, and non-cell-harming alternative to classical separation methods. The separation process relies on a selective physical barrier (membrane) and is conducted without elevated temperatures or an additional extraction phase, making it particularly attractive for recovering thermolabile products and in combination with bioprocesses [40]. Organic polymer membranes are favored due to their cost-efficient fabrication, operability at low temperatures, excellent performance, and good chemical and mechanical properties [41]. Dense membranes are preferred over microporous ones to mitigate the risk of biofouling and pore-clogging [42]. This is particularly

Figure 2

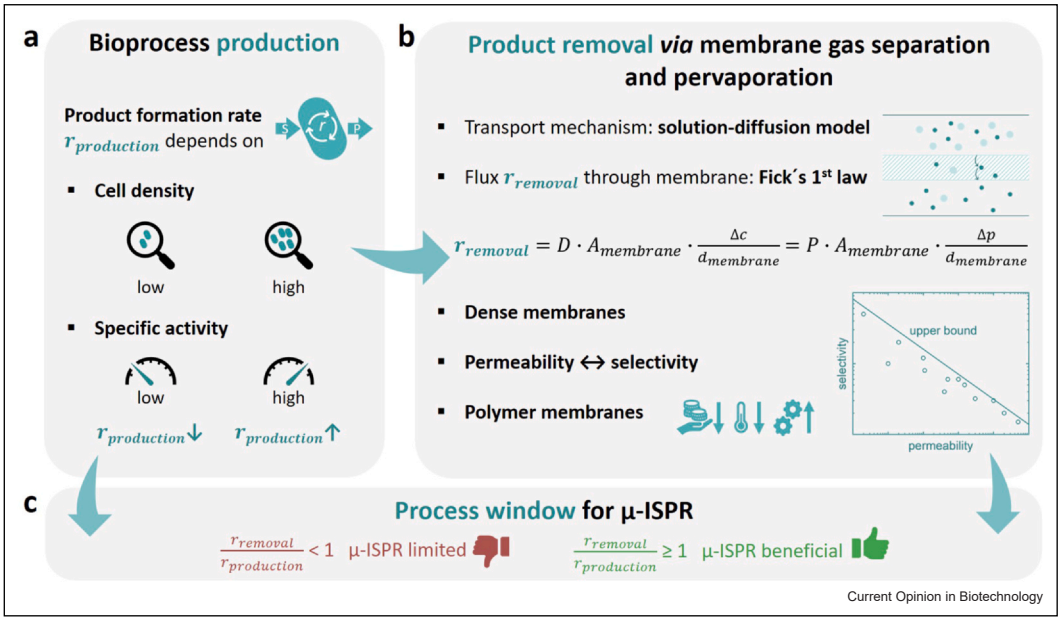

Schematic illustrating the connection between the product formation rate $r_{production}$ of a bioprocess **(a)** and the product removal rate $r_{removal}$ via membrane gas separation and pervaporation **(b)**, highlighting the key parameters for the estimation of the process window for microscale *in-situ* product recovery (µ-ISPR) **(c)**. Overall yield of product over substrate by *in-situ* product recovery is maximized for $\frac{r_{removal}}{r_{production}} \geq 1$ (green thumb up) and limited by mass transfer over the membrane for $\frac{r_{removal}}{r_{production}} < 1$ (red thumb down).

important for immobilized biocatalysts and biofilm applications.

Mass transport through a dense membrane is described by the solution-diffusion model [43]. For membrane transport, an interfacial equilibrium between the membrane material and the fluids on either side is assumed for simplicity. This leads to a continuous chemical potential gradient across the membrane, with interfacial adsorption and desorption being considerably faster than diffusion through the membrane. Therefore, the product removal rate $r_{removal}$ correlates with the diffusion rate $r_{diffusion}$ through the membrane. This is described by Fick's 1st law, with D being the diffusion coefficient, $A_{membrane}$ the membrane area, Δc the concentration gradient, and $d_{membrane}$ the membrane thickness [44]. For the purposes of this study, an extended version of Fick's law was employed, incorporating the permeability coefficient P and the partial pressure gradient Δp as the driving force.

$$r_{removal} = r_{diffusion} = D \cdot A_{membrane} \cdot \frac{\Delta c}{d_{membrane}} = P \cdot A_{membrane} \cdot \frac{\Delta p}{d_{membrane}} \quad (1)$$

Key factors enhancing the product removal rate are a high permeation coefficient P of the membrane material, a large concentration or partial pressure gradient between feed and permeate side, a low membrane thickness $d_{membrane}$, and a high membrane area $A_{membrane}$. The latter two can be optimized by miniaturizing membrane-assisted liquid–gas separation to a microfluidic environment. The sum of partial pressures sets physical limits on the total membrane pressure drop and acts as an additional driving force for maximizing gas transfer rates. Applications of such pressure drops may be limited by mechanical membrane stability. Membrane permeability P is a material constant depending on the characteristics of the material, the permeating compound, and temperature. Hydrophobicity and functional groups affect the affinity, solubility, and interactions of a permeating compound, resulting in different permeabilities of a membrane for different compounds and vice versa. For example, the permeability of PDMS to different gases at 35 °C decreases in the order CO_2 (3.800 Barrer) > H_2 (890 Barrer) > O_2 (800 Barrer) [45]. Membrane permeability and selectivity are inversely related, as illustrated by the Robeson plot (Figure 2b) [46]. Current membrane research is targeting performance optimization using machine learning [47] and mixed-matrix materials [48].

Figure 3

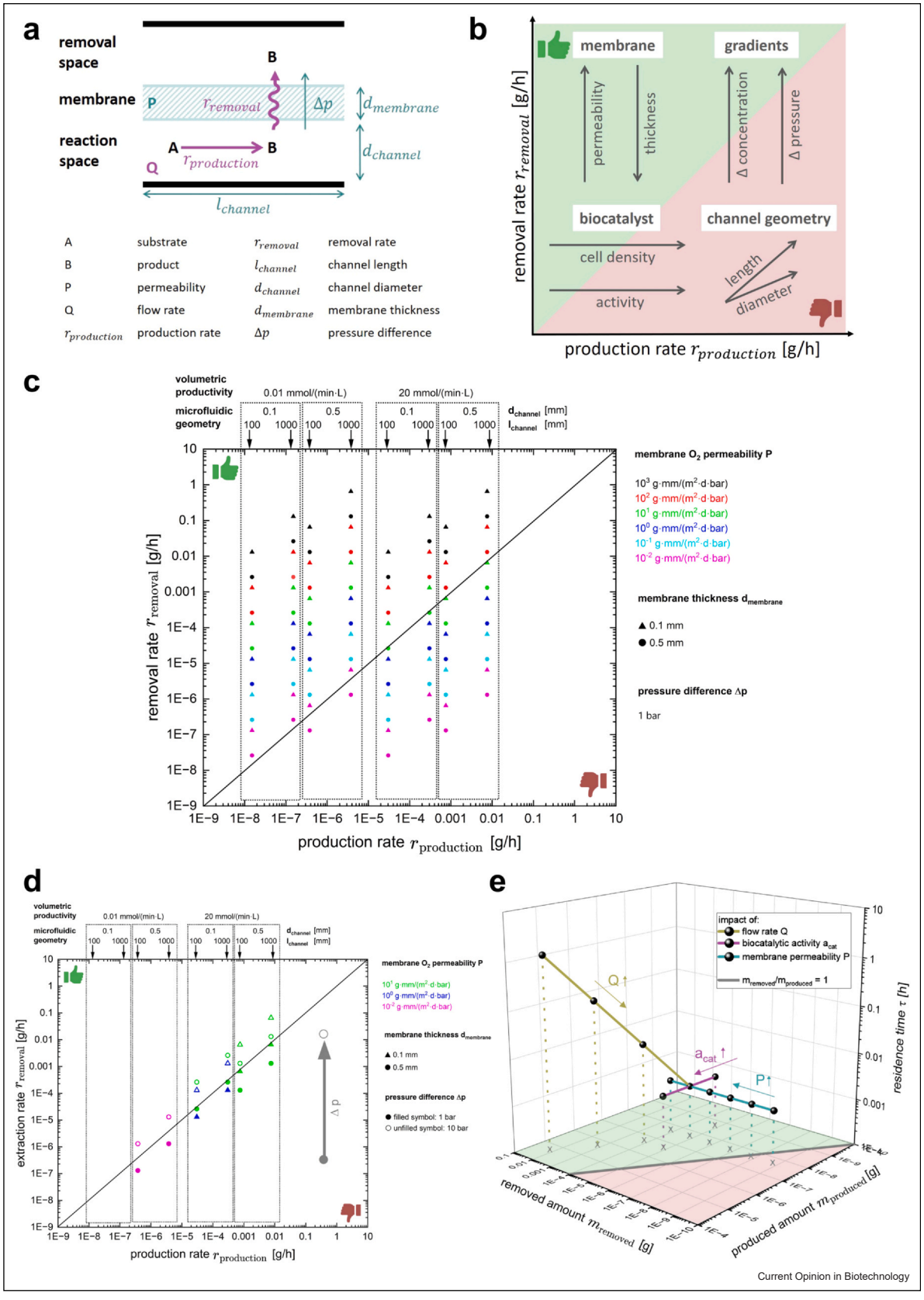
a
removal space
membrane
reaction space
B
P
$r_{removal}$
Δp
$d_{membrane}$
A
B
$r_{production}$
Q
$d_{channel}$
$l_{channel}$
A substrate
B product
P permeability
Q flow rate
$r_{production}$ production rate
$r_{removal}$ removal rate
$l_{channel}$ channel length
$d_{channel}$ channel diameter
$d_{membrane}$ membrane thickness
Δp pressure difference
b
membrane
gradients
permeability
thickness
Δ concentration
Δ pressure
biocatalyst
channel geometry
cell density
activity
length
diameter
removal rate $r_{removal}$ [g/h]
production rate $r_{production}$ [g/h]
c
volumetric productivity
0.01 mmol/(min·L)
20 mmol/(min·L)
microfluidic geometry
$d_{channel}$ [mm]
$l_{channel}$ [mm]
membrane O_2 permeability P
10^3 g·mm/(m²·d·bar)
10^2 g·mm/(m²·d·bar)
10^1 g·mm/(m²·d·bar)
10^0 g·mm/(m²·d·bar)
10^{-1} g·mm/(m²·d·bar)
10^{-2} g·mm/(m²·d·bar)
membrane thickness $d_{membrane}$
▲ 0.1 mm
● 0.5 mm
pressure difference Δp
1 bar
removal rate $r_{removal}$ [g/h]
production rate $r_{production}$ [g/h]
d
extraction rate $r_{removal}$ [g/h]
production rate $r_{production}$ [g/h]
Δ p
● filled symbol: 1 bar
○ unfilled symbol: 10 bar
e
impact of:
flow rate Q
biocatalytic activity a_{cat}
membrane permeability P
$m_{removed}/m_{produced}$ = 1
Q ↑
a_{cat} ↑
P ↑
removed amount $m_{removed}$ [g]
produced amount $m_{produced}$ [g]
residence time τ [h]
Current Opinion in Biotechnology

Representative analysis of simulated microfluidic production and *in-situ* product recovery for the production of O_2 or H_2 using cyanobacteria. **(a)** Schematic top view of the microscale-channel indicating process parameters (blue) and rates (purple) for μ-ISPR. **(b)** Parameter space for the process window emphasizing the influence of different impact factors (membrane-related, channel geometry-related, bioproduction-related) on the applicability of μ-ISPR. **(c)** Simulated data of production and extraction rates ranging for a multitude of impact factors, at Δp = 1 bar. Suitability is shown by division of the dataset by the black line indicating $\frac{r_{removal}}{r_{production}} = 1$. **(d)** Zoomed-in simulated data from panel **(c)** presents the impact of pressure (differences) between reaction and extraction space, applying a 10× higher pressure gradient as driving force. Black line indicates $\frac{r_{removal}}{r_{production}} = 1$. **(e)** Simulated data depicting the impact of residence time τ on the absolute masses in dependence on flow rate, biological activity, and membrane permeability. Gray line implicates the boundary between applicable (green) and non-applicable (red) parameter combinations. The microfluidic dimensions were defined as follows: channel diameter $d_{channel}$ ranging from 100 μm to 500 μm, the channel length $l_{channel}$ ranging from 10 cm to 100 cm. The volumes of the microfluidic reactors were calculated using $V_{microfluidic} = \pi \cdot \left(\frac{d_{channel}}{2}\right)^2 \cdot l_{channel}$. The membrane areas were calculated using $A_{membrane} = 2 \cdot \pi \cdot \frac{d_{channel}}{2} \cdot l_{channel}$, assuming that the channel has a cylindrical shape and the channel wall is the membrane. O_2 production rates $r_{production}$ were estimated by $r_{production} = r_{productivity}^{volumetric} \cdot V_{microfluidic}$, setting $r_{productivity}^{volumetric}$ as 0.01 mmol·min^{-1}·L^{-1} and 20 mmol·min^{-1}·L^{-1}. O_2 removal rates $r_{removal}$ were calculated using $r_{removal} = P \cdot A_{membrane} \cdot \frac{\Delta p}{d_{membrane}}$, setting $d_{membrane}$ as 0.1 mm and 0.5 mm and the O_2 permeabilities P as ranging from 10^{-2} to 10^3 g O_2·mm·m^{-2}·d^{-1}·bar^{-1}. The residence time was calculated using $\tau = \frac{V_{microfluidic}}{Q}$, where Q is the flow rate ranging from 100 nL/min to 100 μL/min. The produced mass $m_{produced}$ and the removed mass $m_{removed}$ were determined by $m_{produced} = r_{production} \cdot \tau$ and $m_{removed} = r_{removal} \cdot \tau$, respectively.

We now conduct a case study on O_2 production in *Synechocystis* and its recovery to assess the feasibility of membrane-based μ-ISPR by comparing $r_{production}$ and $r_{removal}$ of O_2 and defining a process window that satisfies both microfluidic design and biocatalytic requirements (Figure 3, Tables S1-S7). This system serves as a general model adaptable to other reactions and products. It describes an application of membrane-based μ-ISPR for the biotechnological production of O_2, for example, in self-contained environments like an outer space station or the production of H_2 using cyanobacteria [49]. As the hydrogenase involved is inactivated by photosynthetically produced O_2, efficient removal of O_2 is essential to stabilize the hydrogenase reaction, while maintaining high light penetration [50]. Microfluidics or capillaries are therefore the reactor of choice, as the process is not feasible in a tank reactor. Their potential was demonstrated recently for a microfluidic platform enabling precise, high-throughput measurements of cyanobacterial growth at single-cell resolution under controlled light and CO_2 conditions [51].

We simulate the theoretical process window (Figure 3c) using volumetric productivities of 0.01–20 mmol·min^{-1}·L^{-1} as the frame for the biocatalyst [38] (Table S2). O_2 production rates were calculated based on achieved biocatalytic volumetric productivities of *Syn.* sp. PCC 6803, ranging from 77 μmol O_2·min^{-1}·L^{-1} (5 g_{CDW}·L^{-1}) to 12.2 O_2·min^{-1}·L^{-1} (75 g_{CDW}·L^{-1}) [52, 53], which is well within the reported frame (Table S5). The $r_{removal}$ values were calculated for a membrane thickness $d_{membrane}$ of 0.1 mm and 0.5 mm and O_2 permeabilities between 10^{-2} to 10^3 g O_2·mm·m^{-2}·d^{-1}·bar^{-1} (Table S6), covering the range for polymeric membranes and microfluidic materials (Table S3). Figure 3a illustrates the microfluidic device with typical dimensions (channel diameter $d_{channel}$, channel length $l_{channel}$), which were used to calculate channel volumes $V_{microfluidic}$ and membrane areas $A_{membrane}$ (Table S4). Flow rates in the range of 100 nL·min^{-1} to 100 μL·min^{-1} were included; the resulting residence times τ of a reactor volume span 0.47 s to 32.7 h (Table S7). Figure 3b emphasizes qualitatively the influence of the aforementioned parameters on $r_{production}$ and $r_{removal}$, while calculated values for distinct scenarios are provided in Figure 3c–e and visualize the resulting process window (window 1: $r_{production}$ vs. $r_{removal}$). In our case study, $r_{production}$ increases proportional to $l_{channel}$ and $d_{channel}^2$, while $r_{removal}$ increases proportional to $l_{channel}$, $d_{channel}$, $\frac{1}{d_{membrane}}$, P and Δp. The black line dividing the graphs represents the boundary, where $\frac{r_{removal}}{r_{production}} = 1$, indicating μ-ISPR is beneficial for values above this line, but limited below. A shift to the beneficial range can be achieved, for example, by maintaining the setup but increasing the pressure gradient Δp (Formula 1), demonstrated for selected scenarios in Figure 3d (Table S8). Figure 3e highlights simulated data points depicting the impact of the residence time τ on the absolute masses $m_{produced}$ and $m_{removed}$ for a particular combination of parameters (Table S7). The correlation is a complex interplay involving geometric constraints, biocatalytic activity, and permeability. Optimizing these parameters within the boundaries of our case study could allow production of 12.3 O_2 within 3.3 h for a flow rate of 1 μL·min^{-1}, while the recovery could manage 214.2 mg O_2. This illustrates the complexity of parameters to be balanced for an economically feasible process. For a hypothetical process with a product of MW = 100 g·mol^{-1} and $r_{removal} = r_{production}$, the same optimization would lead to the production of 77 mg product within 3.3 h for the same flow rate (Table S7). This indicates that production in microfluidic bioreactors with integrated ISPR is limited to small product quantities in the milligram to lower gram range.

In total, this identifies requirements for biocatalyst, membrane material, and microfluidic layout of μ-ISPR in bioprocesses, defining the frame for future microfluidic bioprocess design. The μ-ISPR process window is

Figure 4

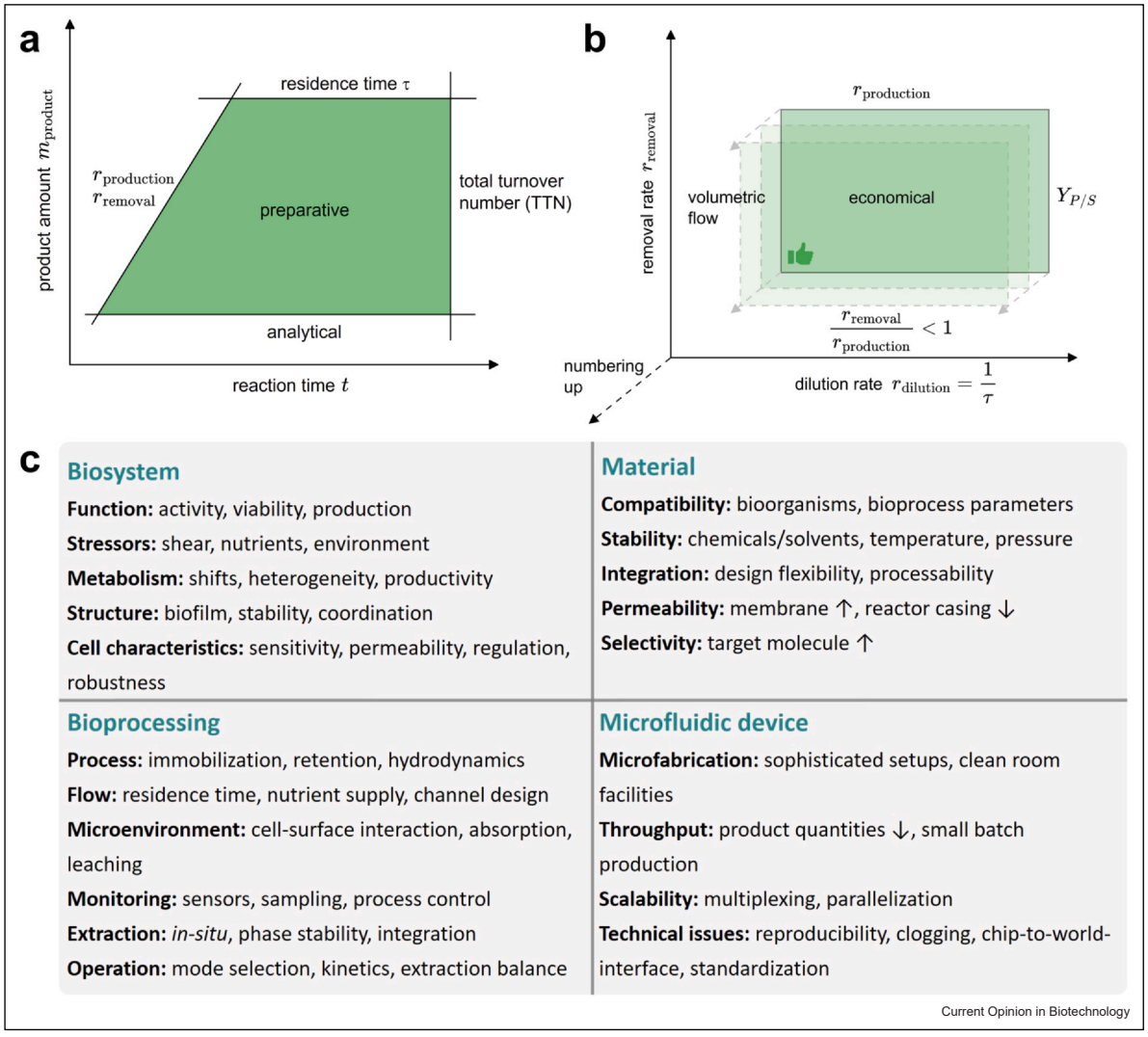

Biological and technical challenges regarding the process window for a feasible preparative application using microfluidic *in-situ* product recovery. **(a)** Process window of a preparative μ-ISPR determined by adjustable process parameters. **(b)** Opportunities to expand production by numbering up. **(c)** Overview of highly influential process parameters, which have to be considered when designing a μ-ISPR process.

governed by the interplay between the biocatalytic system, device geometry, and material properties, balancing production and removal rates within given residence times. Maximum efficiency is theoretically achieved when $r_{removal} \geq r_{production}$, assuming complete product conversion to define an ideal process window (Figure 3e, green), with product amounts in the mg range per channel (Table S7). Practically, biological, process, and microfluidic constraints affect production, removal rates, and residence times. Thus, the technical and economic feasibility of μ-ISPR must be evaluated individually for each biocatalytic system and microfluidic setup, depending on its final application.

Challenges of productive μ-ISPR systems

lProductive μ-ISPR operation is confined to a narrow process window defined by residence time, catalyst stability, production rate, and product removal performance. Balancing these constraints with technological opportunities establishes a distinct process window in which whole-cell bioproduction approaches industrially relevant output [5, 37]. Overall productivity (total mass per time) arises from the interplay of specific production and removal rate with effective residence time and total turnover number, distinguishing analytical demonstrations from preparative applications based on total product amounts $m_{product}$ within the process window (Figure 4a). Product

residence time limits are mainly governed by membrane permeability and mass-transfer characteristics, while production depends on biocatalytic properties and microfluidic compatibility.

Feasibility requires balancing volumetric productivity, removal rate, and absolute product yield under membrane- and mass transfer-limited residence times within the process window. Excessively high production rates exceed ISPR capacity due to diffusion and permeability limits, while overly slow production yields insufficient overall productivity to justify μ-ISPR economically (Figure 4b). Productivity gains cannot be realized by extending channel length or residence time alone, as microscale hydrodynamics and catalyst lifetime impose strict limits. Consequently, expanding the process window towards economically attractive bioprocessing relies almost exclusively on numbering-up strategies that replicate optimized microreactor units while preserving flow regimes and separation performance (Figure 4b).

Within this constrained space, μ-ISPR performance emerges from the tight coupling of biosystem, bioprocessing, material selection, and microfluidic device design, defining robustness, reproducibility, and scalability (Figure 4c). Miniaturization amplifies interdependencies and shifts optimization towards system-level co-design.

The biosystem demands metabolic activity, viability, and regulatory stability at high cell densities for continuous productivity. Microscale confinement increases mechanical stress, plug-flow induced nutrient gradients, and metabolite accumulation, causing metabolic heterogeneity and productivity drifts. Strain-specific factors such as shear tolerance, secretion behavior, and adhesion might complicate cell retention, spatial organization, recovery efficiency, and long-term operation.

Bioprocessing in μ-ISPR necessitates precise coordination of immobilization, hydrodynamics, and *in-situ* recovery. The flow governs residence time, nutrient supply, and space-time yield, but excessive shear or dilution undermines retention and functional compartmentalization [54]. Integrating production with recovery demands matching kinetics without cross-interference [13]. Channel geometry and microscale transport phenomena modulate cell-surface interactions, adsorption, and leaching [55], while limited sensor integration necessitates reliance on intrinsic process stability [20, 56].

Materials must balance biocompatibility, ISPR compatibility, and fabrication requirements, supporting cell viability while tolerating ISPR conditions. Membranes should provide high permeability and selectivity, while reactor barriers must prevent product loss. Membrane development involves the design of materials with exceedingly high permeabilities and materials with a high selectivity for a target compound. A crucial challenge is to identify the optimal balance, the 'sweet spot', for a particular application. Elastomers and photopolymers enable flexible integration and rapid prototyping but limit biocompatibility and long-term stability, whereas low-permeability thermoplastics and glass provide robust containment. These trade-offs motivate multi-material architectures by decoupling reaction and separation [57, 58].

Microfluidic device performance is dominated by fabrication complexity [59], limited throughput, and operational robustness. Small volumes and restricted residence times confine μ-ISPR to low-to-moderate production scales, with up-scaling achieved via parallelization, increasing system complexity [18, 60], and risks such as clogging, fouling, and pressure instability. Predictive modeling is essential to balance channel dimensions, hydrodynamics, and biological constraints within a tightly bounded feasible operating space [5, 15].

Feasible applications and product classes cover high-value and low-quantity products, such as pharmaceutical (intermediate) products, specialty chemicals, derivatives of natural substances, and diagnostic reagents. Process productivity significantly affects the cost-benefit ratio and thus the technical and economic feasibility of an application. Conceptual product classes include fine chemicals or products from modular, decentralized processes, for example, for direct downstream use or for removing reactants inhibiting the target reaction.

Concluding remarks and future perspectives

Productive μ-ISPR systems based on membrane separation are not suitable for all biocatalysts or process control strategies. Of interest are high-value, low-quantity products for which their application might be technically feasible and economically advantageous. Based on economically relevant industrial production rates, product quantities in the milligram to gram range may be achieved for small molecules in production times of up to several hours, constrained by practical retention times in single microcapillaries. These values are consistent with experimental results of initial studies of productive microsystems for different model compounds at the laboratory microscale. It is important to emphasize that these volumetric productivities of 20 $mmol \cdot min^{-1} \cdot L^{-1}$ correspond to high total turnover numbers and represent exceptionally high and challenging benchmarks. Even with advanced metabolic and enzyme engineering, achieving such performance remains highly unlikely for enzymes with turnover rates K_{cat} below $10\,s^{-1}$. Numbering up by a factor of 1000 may be technically achievable, enabling higher gram amounts of total product per day in microfluidic membrane-based ISPR, provided that challenges for maximizing biosystem

efficiency and material compatibility in given geometries are met. This also provides strong arguments for expanding analytical applications towards fermentations in microfluidic formats with integrated ISPR into the realm of preparative microfluidic fermentations for selected examples and limited amounts of product. The arguments presented here for model cases of aqueous-gas reactions can be adapted to all other ISPR concepts in bioprocesses, depending on reaction rates and times of respective biocatalysts, reactor geometries, and mass transfer. Higher space-time yields may be achieved in ISPR formats with slug flow, where the permeabilities of interfaces are more favorable. The μ-ISPR process window concepts discussed here can also be used for productive microfluidic bioprocesses in general. Practical limitations of numbering-up, catalytic volumetric turnover rates, mass transfer, and reactor geometries are thus likely to confine the productivity of microfluidic bioprocesses to higher gram amounts of products, supporting decentralized application cases or access to products that are otherwise inaccessible.

Funding
The infrastructure at the UFZ was funded by H2Saxony Grant no. 100361842.

Author contributions
Corinna Golze: Conceptualization, Investigation, Synthesis, Visualization, Writing – original draft, review, editing. **Claudia Hackl:** Conceptualization, Investigation, Synthesis, Visualization, Writing – original draft, review, editing. **Alexander Grünberger:** Writing – review & editing. **Andreas Schmid:** Conceptualization, Synthesis, Visualization, Writing – original draft, review, editing, Project management.

Data Availability
The data are available as supplementary data (S1-S8).

Declaration of Competing Interest
The authors declare no conflict of interest.

Declaration of Generative AI and AI-assisted technologies in the writing process
During the preparation of this work, the author(s) used ChatGPT 5.2 to assist in improving the clarity, grammar, and style of the manuscript. After using these tools, the author(s) thoroughly reviewed and edited the content as needed and take full responsibility for the content of the published article.

Appendix A. Supplementary data
Supplementary data (S1-S8) associated with this article can be found in the online version at doi:10.1016/j.copbio.2026.103498.

References and recommended reading
Papers of particular interest, published within the period of review, have been highlighted as:

- • of special interest
- •• of outstanding interest

1. Lye GJ, Woodley JM: **Application of in situ product-removal techniques to biocatalytic processes**. *Trends Biotechnol* 1999, **17**:395-402.

2. Stark D, von Stockar U: **In situ product removal (ISPR) in whole cell biotechnology during the last twenty years**. *Adv Biochem Eng Biotechnol* 2003, **80**:149-175.

3. Outram V, Lalander C-A, Lee JGM, Davies ET, Harvey AP: **Applied in situ product recovery in ABE fermentation**. *Biotechnol Prog* 2017, **33**:563-579.

4. van Hecke W, Kaur G, De Wever H: **Advances in in-situ product recovery (ISPR) in whole cell biotechnology during the last decade**. *Biotechnol Adv* 2014, **32**:1245-1255.

5. •• Scholz Y, Yermakov B, Grünberger A: **Windows of operation as qualitative early-stage design tool for microfluidic (single-cell) cultivations**. *Curr Opin Biotechnol* 2025, **97**:103401.
Excellent qualitative framework highlighting the window of operation concept as beneficial design tool for microfluidic cultivation.

6. Woodley JM: **Biocatalysis in microfluidic systems: an experimental basis for data science**. *React Chem Eng* 2024, **9**:2028-2033.

7. Marks DM: **Equipment design considerations for large scale cell culture**. *Cytotechnology* 2003, **42**:21-33.

8. Wang GR, Yang F, Zhao W: **There can be turbulence in microfluidics at low Reynolds number**. *Lab Chip* 2014, **14**:1452-1458.

9. Karande R, Schmid A, Buehler K: **Applications of multiphasic microreactors for biocatalytic reactions**. *Org Process Res Dev* 2016, **20**:361-370.

10. Boodhoo K, Flickinger MC, Woodley JM, Emanuelsson E: **Bioprocess intensification: a route to efficient and sustainable biocatalytic transformations for the future**. *Chem Eng Process Process Intensif* 2022, **172**:108793.

11. Heintz S, Börner T, Ringborg RH, Rehn G, Grey C, Nordblad M, Krühne U, Gernaey KV, Adlercreutz P, Woodley JM: **Development of in situ product removal strategies in biocatalysis applying scaled-down unit operations**. *Biotechnol Bioeng* 2017, **114**:600-609.

12. Žnidaršič-Plazl P, Plazl I: **Modelling and experimental studies on lipase-catalyzed isoamyl acetate synthesis in a microreactor**. *Process Biochem* 2009, **44**:1115-1121.

13. Heintz S, Mitic A, Ringborg RH, Krühne U, Woodley JM, Gernaey KV: **A microfluidic toolbox for the development of in-situ product removal strategies in biocatalysis**. *J Flow Chem* 2016, **6**:18-26.

14. Zhang Y, Benes NE, Lammertink RG: **Performance study of pervaporation in a microfluidic system for the removal of acetone from water**. *J Chem Eng* 2016, **284**:1342-1347.

15. •• Potočnik H, Šmigoc Y, Plazl I, Plazl PŽ, Ambrožič R: **Model-based design of a microfluidic pervaporation device for intensified VOC separation**. *Sep Purif Technol* 2025, **378**:134795.
Excellent study on a model-guided design of a microfluidic device for highly efficient membrane-based μ-ISPR.

16. Posten C: **Design principles of photo-bioreactors for cultivation of microalgae**. *Eng Life Sci* 2009, **9**:165-177.

17. Hoschek A, Heuschkel I, Schmid A, Bühler B, Karande R, Bühler K: **Mixed-species biofilms for high-cell-density application of *Synechocystis* sp. PCC 6803 in capillary reactors for continuous cyclohexane oxidation to cyclohexanol**. *Bioresour Technol* 2019, **282**:171-178.

18. Tamborini L, Fernandes P, Paradisi F, Molinari F: **Flow bioreactors as complementary tools for biocatalytic process intensification**. *Trends Biotechnol* 2018, **36**:73-88.

19. Hollmann L, Blank LM, Grünberger A: **Flow fermentation: microsystems for whole-cell bioproduction processes**. *Trends Biotechnol* 2025, **43**:1528-1539.

20. Alpural A, Kimiz-Gebologlu I, Parekh M, Imamoglu E, Ali Z, Yesil-Celiktas O: **Systematic review on the role of microfluidic platforms in advancing scalable and precise microbial bioprocessing**. *Eng Life Sci* 2025, **25**:e70034.

21. Ham S, Kim HJ, Shin N, Hwang JH, Oh SJ, Park JY, Joo JC, Kim HT, Bhatia SK, Yang Y-H: **Continuous production of gamma aminobutyric acid by engineered and immobilized *Escherichia coli* whole-cells in a small-scale reactor system**. *Enzym Microb Technol* 2023, **168**:110258.

22. Menegatti T, Žnidaršič-Plazl P: **Copolymeric hydrogel-based immobilization of yeast cells for continuous biotransformation of fumaric acid in a microreactor**. *Micromachines* 2019, **10**:867.

23. Peschke T, Bitterwolf P, Hansen S, Gasmi J, Rabe KS, Niemeyer CM: **Self-immobilizing biocatalysts maximize space–time yields in flow reactors**. *Catalysts* 2019, **9**:164.

24. Kronstadt SM, Patel DB, Born LJ, *et al.*: **Mesenchymal stem cell culture within perfusion bioreactors incorporating 3D-printed scaffolds enables improved extracellular vesicle yield with preserved bioactivity**. *Adv Health Mater* 2023, **12**:e2300584.

25. • Lemke P, Schneider L, Kunz W, Rieck AL, Jäger PS, Bruckmann A, Nestler B, Rabe KS, Niemeyer CM: **Flow-induced microfluidic assembly for advanced biocatalysis materials**. *Adv Funct Mater* 2024, **34**:2313944.

Demonstration of a continuous microfluidic bioreactor with immobilized cells for long-term cultivation while maintaining extraordinarily high space–time yields.

26. • Bajić M, Khiawjan S, Hilton ST, Lye GJ, Marques MP, Szita N: **A paradigm shift for biocatalytic microreactors: decoupling application from reactor design**. *Biochem Eng J* 2024, **205**:109260.

Demonstration of a flexible microreactor platform for versatile biocatalytic applications involving enzymes to whole cells.

27. Salas-Villalobos UA, Gómez-Acata RV, Castillo-Reyna J, Aguilar O: **In situ product recovery as a strategy for bioprocess integration and depletion of inhibitory products**. *J Chem Technol Biotechnol* 2021, **96**:2735-2743.

28. Wohlgemuth R, Plazl I, Žnidaršič-Plazl P, Gernaey KV, Woodley JM: **Microscale technology and biocatalytic processes: opportunities and challenges for synthesis**. *Trends Biotechnol* 2015, **33**:302-314.

29. Bekavac N, Benković M, Jurina T, Valinger D, Gajdoš Kljusurić J, Jurinjak Tušek A, Šalić A: **Advancements in aqueous two-phase systems for enzyme extraction, purification, and biotransformation**. *Molecules* 2024, **29**:3776.

30. Santos AG, Albuquerque TL, de, Ribeiro BD, Coelho MAZ: **In situ product recovery techniques aiming to obtain biotechnological products: a glance to current knowledge**. *Biotechnol Appl Biochem* 2021, **68**:1044-1057.

31. Bacchin P, Leng J, Salmon J-B: **Microfluidic evaporation, pervaporation, and osmosis: from passive pumping to solute concentration**. *Chem Rev* 2022, **122**:6938-6985.

32. Ziemecka I, Haut B, Scheid B: **Continuous separation, with microfluidics, of the components of a ternary mixture: from vacuum to purge gas pervaporation**. *Microfluid Nanofluid* 2017, **21**:84.

33. Zizzari A, Bianco M, Perrone E, *et al.*: **Microfluidic pervaporation of ethanol from radiopharmaceutical formulations**. *Chem Eng Process Process Intensif* 2019, **141**:107539.

34. • Wahab MA, Domingues C, Azevedo AM, Chu V, Conde JP, Aires-Barros MR: **An integrated microfluidic device for continuous bioprocessing**. *Sep Purif Technol* 2024, **332**:125702.

Remarkable example of a fully integrated continuous microfluidic platform combining bioproduction and μ-ISPR.

35. Toepel J, Karande R, Bühler B, Bühler K, Schmid A: **Photosynthesis driven continuous hydrogen production by diazotrophic cyanobacteria in high cell density capillary photobiofilm reactors**. *Bioresour Technol* 2023, **373**:128703.

36. Zhou YH, Titchener-Hooker NJ: **Visualizing integrated bioprocess designs through? Windows of operation?** *Biotechnol Bioeng* 1999, **65**:550-557.

37. Woodley JM, Titchener-Hooker NJ: **The use of windows of operation as a bioprocess design tool**. *Bioprocess Eng* 1996, **14**:263-268.

38. • Hauer B: **Embracing nature's catalysts: a viewpoint on the future of biocatalysis**. *ACS Catal* 2020, **10**:8418-8427.

Excellent overview of quantitative factors and needs for industrialization of biocatalytic processes.

39. Straathof AJJ, Panke S, Schmid A: **The production of fine chemicals by biotransformations**. *Curr Opin Biotechnol* 2002, **13**:548-556.

40. Castro-Muñoz R: **Membranes– future for sustainable gas and liquid separation?** *Curr Res Green Sustain Chem* 2022, **5**:100326.

41. Sidhikku Kandath Valappil R, Ghasem N, Al-Marzouqi M: **Current and future trends in polymer membrane-based gas separation technology: a comprehensive review**. *J Ind Eng Chem* 2021, **98**:103-129.

42. Elisiário MP, Wever H, de, van Hecke W, Noorman H, Straathof AJJ: **Membrane bioreactors for syngas permeation and fermentation**. *Crit Rev Biotechnol* 2022, **42**:856-872.

43. Wijmans JG, Baker RW: **The solution-diffusion model: a review**. *J Membr Sci* 1995, **107**:1-21.

44. Fuchs G: **Allgemeine Mikrobiologie**; 2007.

45. Merkel TC, Bondar VI, Nagai K, Freeman BD, Pinnau I: **Gas sorption, diffusion, and permeation in poly(dimethylsiloxane)**. *J Polym Sci B Polym Phys* 2000, **38**:415-434.

46. Robeson LM: **Correlation of separation factor versus permeability for polymeric membranes**. *J Membr Sci* 1991, **62**:165-185.

47. Yang J, Tao L, He J, McCutcheon JR, Li Y: **Machine learning enables interpretable discovery of innovative polymers for gas separation membranes**. *Sci Adv* 2022, **8**:eabn9545.

48. Qian Q, Asinger PA, Lee MJ, Han G, Mizrahi Rodriguez K, Lin S, Benedetti FM, Wu AX, Chi WS, Smith ZP: **MOF-based membranes for gas separations**. *Chem Rev* 2020, **120**:8161-8266.

49. Bühler K, Bühler B, Klähn S, Krömer JO, Dusny C, Schmid A: **11 Biocatalytic production of white hydrogen from water using cyanobacteria**. In *Photosynthesis: Biotechnological Applications with Microalgae*. Edited by Rögner M. De Gruyter; 2021:279-306.

50. McIntosh CL, Germer F, Schulz R, Appel J, Jones AK: **The NiFe-hydrogenase of the cyanobacterium *Synechocystis* sp. PCC 6803 works bidirectionally with a bias to H_2 production**. *J Am Chem Soc* 2011, **133**:11308-11319.

51. Witting L, Seiffarth J, Stute B, Schulze T, Hofer JM, Nöh K, Eisenhut M, Weber APM, Lieres E von, Kohlheyer D: **A microfluidic system for the cultivation of cyanobacteria with precise light intensity and CO_2 control: enabling growth data acquisition at single-cell resolution**. *Lab Chip* 2025, **25**:319-329.

52. Zavřel T, Očenášová P, Červený J: **Phenotypic characterization of *Synechocystis* sp. PCC 6803 substrains reveals differences in sensitivity to abiotic stress**. *PLoS One* 2017, **12**:e0189130.

53. Grund M, Jakob T, Toepel J, Schmid A, Wilhelm C, Bühler B: **Heterologous lactate synthesis in *Synechocystis* sp. Strain PCC 6803 causes a growth condition-dependent carbon sink effect**. *Appl Environ Microbiol* 2022, **88**:e0006322.

54. Huber D, Oskooei A, Casadevall I, Solvas X, Andrew D, Kaigala GV: **Hydrodynamics in cell studies**. *Chem Rev* 2018, **118**:2042-2079.

55. Carter S-SD, Atif A-R, Kadekar S, Lanekoff I, Engqvist H, Varghese OP, Tenje M, Mestres G: **PDMS leaching and its implications for on-chip studies focusing on bone regeneration applications**. *Organs-on-Chip* 2020, **2**:100004.

56. Marques MP, Szita N: **Bioprocess microfluidics: applying microfluidic devices for bioprocessing**. *Curr Opin Chem Eng* 2017, **18**:61-68.

57. Nielsen JB, Hanson RL, Almughamsi HM, Pang C, Fish TR, Woolley AT: **Microfluidics: innovations in materials and their fabrication and functionalization**. *Anal Chem* 2020, **92**:150-168.

58. Adewole JK, Owoyale FB, Oladipo HB, Ahmed AL: **Membrane pervaporation technology for the separation of organic liquids from water: a review of advancements in material modification and membrane fabrication**. *Research* 2025, **2**:100914.

59. Scott SM, Ali Z: **Fabrication methods for microfluidic devices: an overview**. *Micromachines* 2021, **12**:319.

60. Su Y, Kuijpers K, Hessel V, Noël T: **A convenient numbering-up strategy for the scale-up of gas–liquid photoredox catalysis in flow**. *React Chem Eng* 2016, **1**:73-81.